Green Chemistry

PAPER

View Article Online
View Journal | View Issue



Cite this: *Green Chem.*, 2025, **27**, 6869

# Platinum nanoparticle-doped recycled PLA filament for sustainable additive manufactured electrocatalytic architectures†

Karen K. L. Augusto, [a,b] Robert D. Crapnell, [a] Elena Bernalte, [a] Hayley G. Andrews,[a] Orlando Fatibello-Filho [b] and Craig E. Banks *[a]

Additive manufacturing has the ability to facilitate the fabrication of advanced electrochemical architectures. To truly realise this, bespoke and high-performance filaments must be realised. This study presents a sustainable approach for developing highly conductive filament doped with platinum nanoparticles (PtNPs) and characterises them towards the hydrogen evolution reaction (HER). The PtNPs were synthesised using a green methodology, utilising aqueous conditions and graphite flakes as the only reducing agent. The PtNP-doped graphite was incorporated into recycled polylactic acid (rPLA)-based filaments, enabling the fabrication of highly conductive electrodes with enhanced electrocatalytic properties. The PtNPs-supported graphite (PtNPs-G) material was first characterised using SEM, EDX, XPS, and XRD, confirming the successful deposition of PtNPs. Next, electrochemical studies are performed using cyclic voltammetry, electrochemical impedance spectroscopy, and linear sweep voltammetry, to demonstrate the enhanced electrochemical and electrocatalytic performance of the PtNPs-G electrodes. The optimised PtNPs-G(12%) electrode exhibited a HER onset potential of −0.04 V (*vs.* RHE), a Tafel slope of 46 mV dec$^{-1}$, and an overpotential of −312 mV at 10 mA cm$^{-2}$. Stability tests over 1000 linear sweep voltammetry cycles and 7-hour chronoamperometry demonstrated good durability, although minor performance degradation was attributed to known ingress tendency of the PLA matrix. The findings demonstrate the potential of additive manufacturing fabricated electrocatalysts for sustainable hydrogen production, reducing Pt usage while maintaining their high efficiency. This work highlights the versatility of additive manufacturing in developing cost-effective, customisable, and high-performance electrochemical devices for renewable energy applications.

Received 17th February 2025,
Accepted 16th May 2025

DOI: 10.1039/d5gc00851d

rsc.li/greenchem



## Green foundation

1. Platinum nanoparticles were produced on graphite flakes using an eco-friendly aqueous synthesis and no additional reagents. This was used to make a bespoke filament from recycled PLA and bio-based castor oil, using only 5 minutes of thermal mixing and no solvents. The filament showed excellent printability and performance towards the production of green hydrogen.
2. Sustainably produced PtNP-doped filament provided better HER performance (−0.04 V *vs.* RHE) compared to previously reported filaments and post-print modified electrodes.
3. Future research could focus on improving the loading of PtNPs, considering recycling of the material post-use, and improving the long-term stability of the material.

## 1. Introduction

Hydrogen, a versatile and zero-emission fuel, is key to the clean energy transition, offering immense potential to decarbonise major sectors.[1] Hydrogen ($H_2$) production method is through the conversion of methane ($CH_4$) into hydrogen and carbon monoxide or dioxide, a process known as grey hydrogen production. However, this method is energy-intensive and generates significant greenhouse gas emissions, undermining

[a]*Faculty of Science and Engineering, Manchester Metropolitan University, Dalton Building, Chester Street, M1 5GD, Great Britain. E-mail: c.banks@mmu.ac.uk; Tel: +44(0)1612471196*
[b]*Laboratório de Analítica, Bioanalítica, Biosensores, Electroanalítica e Sensores, Departamento de Química, Universidade Federal de São Carlos (UFSCar), CP 676, 13560-970 São Carlos-SP, Brazil*

† Electronic supplementary information (ESI) available. See DOI: https://doi.org/10.1039/d5gc00851d

its environmental benefits.[2–4] In contrast, green hydrogen has emerged as the ideal alternative, addressing these shortcomings providing a sustainable and environmentally friendly solution, and aligning with the United Nations Sustainable Development Goals, in particular Goal 7 "Affordable and Clean Energy".[5] Hydrogen produced *via* water electrolysis, green hydrogen, is the cleanest form of hydrogen, with zero carbon emissions. This process involves splitting water ($H_2O$) into hydrogen ($H_2$) and oxygen ($O_2$) using electricity in an electrolyser.[2,6] However, large-scale electrochemical water splitting, which involves the hydrogen evolution reaction (HER) and oxygen evolution reaction (OER), is significantly limited with its low efficiency, as both HER and OER require significant overpotentials to proceed at practical rates.[4,7] In this sense, the overall efficiency of the process is determined by the intrinsic electrocatalytic properties of the materials involved.[8]

Platinum (Pt) has been the main catalyst used to support the HER and OER. The main problem associated with this noble metal is the high cost of using Pt-based catalysts.[4] As a result, several research groups have been studying adapted methodologies to try to reduce the cost associated with the use of Pt minimising its usage and enhancing efficiency. Such strategies include alloying with cheaper metals, nano-structuring to increase surface area, and utilising advanced support materials to improve catalyst performance and stability.[9–11] For example, Zhang *et al.* explored a new approach to enhance the efficiency of Pt catalysts for HER immobilising single platinum atoms on MXene, a 2D material, the study demonstrates improved catalytic performance with low overpotentials due to increased active sites and efficient electron transfer.[12] In another work, researchers investigated the use of phosphorus-doped activated carbon (P-AC) as a support for Pt catalysts. They synthesised P-AC introducing phosphorus into activated carbon and then depositing Pt nanoparticles onto this modified support. The results showed that the Pt/P-AC catalyst exhibited superior HER activity compared to Pt supported on undoped activated carbon and demonstrated good stability over multiple cycles, making it promising for practical hydrogen production.[13]

In this context, additive manufacturing has significant potential for sustainabe innovations in this field. It offers important advantages for developing electrocatalytic platforms applicable to hydrogen production facilitating the creation of complex structures and enabling the incorporation of recycled and renewable materials. Moreover, its precise control over electrode design, composition, and architecture allows for optimisation of active site distribution and mass transport, improving the electrocatalytic performance of whole devices.[14–17] Hughes *et al.*[18] investigated additive manufacturing to develop electrocatalytic anodes and cathodes for water splitting incorporating materials 2D-$MoSe_2$, conductive carbon, and Pt/C into PLA filaments, the researchers produced electrodes that exhibited effective hydrogen and oxygen evolution reactions without the necessity for post-production treatments. The results showed that, among the tested materials, the filament containing commercial 20% Pt on carbon (Pt/C) exhibited the highest HER performance, achieving an onset potential of −0.09 V (*vs.* RHE). Despite the promising progress demonstrated in HER with reduced platinum usage, further decreasing platinum loading is crucial for real-world applications due to its high cost and limited availability.[13] Moreover, the use of carbon black raises sustainability concerns, not only due to its sourcing and production impact but also its associated costs.[16,19] To address this challenge, researchers have explored incorporating carbon black with graphite to lower the cost of additive manufactured electrode production while enhancing the material's conductivity.[16,19,20] Further advancing sustainability, Sigley *et al.* (2023)[21] pioneered the use of recycled poly(lactic acid) (PLA) from coffee pods to produce conductive filaments for electroanalytical applications. Additionally, Crapnell *et al.*[15] demonstrated the first electrically conductive additive manufacturing filament utilising castor oil as a bio-based plasticiser. These studies highlight the viability of using recycled, natural, and bio-based materials in additive manufacturing to enhance electrochemical sensing performance while promoting sustainability.

In this regard, integrating green synthesis methods with additive manufacturing-based electrode fabrication presents a promising pathway toward scalable, high-performance, and sustainable HER electrocatalysts. This study focuses on the green synthesis of platinum nanoparticles supported on graphite and their incorporation into conductive additive manufacturing filaments for HER applications. The PtNPs-G-modified electrodes are characterised in terms of physicochemical properties and electrocatalytic activity, providing insights into their potential for hydrogen production *via* electrochemical water splitting leveraging additive manufacturing. This work aims to advance sustainable electrode fabrication, reducing reliance on expensive noble metals while maintaining high HER efficiency.

## 2. Experimental

### 2.1 Chemicals

All chemicals used were of analytical grade and used as received without any further purification. All solutions were prepared with deionised water of resistivity not less than 18.2 MΩ cm from a Milli-Q Integral 3 system from Millipore UK (Watford, UK). Hexaammineruthenium(III) chloride (98%), castor oil, potassium ferricyanide (99%), potassium ferrocyanide (98.5–102.0%), sodium hydroxide (>98%), potassium chloride (99.0–100.5%), potassium hexachloroplatinate(IV) (98%), and sulphuric acid (99.999%) were purchased from Merck (Gillingham, UK). Carbon black (CB) (>99+%) was purchased from PI-KEM (Tamworth, UK) and graphite powder <53 μm was purchased from Inoxia Ltd (Cranleigh, UK). Recycled poly (lactic acid) (rPLA) was purchased from Gianeco (Turin, Italy).

### 2.2 Platinum nanoparticles on graphite production

The graphite modified with platinum nanoparticles (PtNPs) was prepared based on an approach reported previously.[22]

 

Briefly, a 20 mg $mL^{-1}$ platinum solution was prepared and stirred with 20 g of graphite powder overnight. Then, this solution containing graphite and PtNPs was vacuum filtered and allowed to dry in an oven at 60 °C overnight. The resulting powder, labelled PtNPs-G, was used to further filament production.

### 2.3 Filament production

Prior to any mixing or filament production, all rPLA was dried in an oven at 60 °C for a minimum of 2.5 h, which removed any residual water in the polymer. The filament was prepared through the addition of appropriate amounts of rPLA, castor oil, CB, and PtNPs-G in a chamber of 63 $cm^3$. All filaments made throughout this work utilised 10 wt% castor oil as a plasticiser,[15] 60 wt% of PLA, and 30 wt% of carbon loading (CB + PtNPs-G). The compositions of CB and PtNPs-G investigated in this study were as follows: 21 wt% CB + 9 wt% PtNPs-G, 18 wt% CB + 12 wt% PtNPs-G, and 15 wt% CB + 15 wt% PtNPs-G, maintaining a consistent total carbon content of 30 wt%. Additionally, a filament without Pt nanoparticles, non-modified graphite, was prepared with the same carbon loadings as the PtNPs-G filaments. This graphite filament served as a reference for comparative analysis of the electrochemical and electrocatalytic performance against the proposed PtNPs-G filaments. The compounds were mixed at 190 °C with Banbury rotors at 70 rpm for 5 min using a Thermo Haake Polydrive dynameter fitted with a Thermo Haake Rheomix 600 (Thermo-Haake, Germany). The resulting polymer composites were allowed to cool to room temperature before being granulated to create a finer granule size using a Rapid Granulator 1528 (Rapid, Sweden). The granulated sample was collected and processed through the hopper of a EX6 extrusion line (Filabot, VA, United States). The EX6 was set up with a single screw with four set heat zones of 60, 190, 195, and 195 °C, respectively. The molten polymer was extruded from a 1.75 mm die head, pulled along an Airpath cooling line (Filabot, VA, United States), through an inline measure (Mitutoyo, Japan), and collected on a Filabot spooler (Filabot, VA, United States). The filament was then ready to use for additive manufacturing.

### 2.4 Additive manufacturing of the electrodes

All computer designs and .3MF files seen throughout this manuscript were produced using Fusion 360® (Autodesk®, CA, United States). These files were sliced and converted to .GCODE files ready for printing using the printer-specific software, PrusaSlicer (Prusa Research, Prague, Czech Republic). The additive manufactured electrodes were produced using fused filament fabrication (FFF) technology on a Prusa i3 MK3S+ (Prusa Research, Prague, Czech Republic). All electrodes were printed using a 0.6 mm nozzle with a nozzle temperature of 225 °C, extrusion ratio of 1.6 (160%), 100% rectilinear infill,[23] 0.2 mm layer height, print speed of 40 mm $s^{-1}$ and bed temperature of 50 °C.

Please see the ESI† for further information on the physicochemical characterisation and electrochemical experiments.

## 3. Results and discussion

### 3.1 Green synthesis of PtNPs on graphite for filament production and its physicochemical characterization

Due to the practical and sustainable advantages of additive manufacturing, but significant shortcomings in the quality and functionality of commercially available filament, researchers are producing customised filaments for electrode production, emphasising improved conductivity, performance, and sustainability.[24] While carbon black is known for its excellent conductivity, its production poses environmental challenges due to the combustion of petroleum products. Therefore, using eco-friendly alternatives like graphite can enhance filament quality and reduce costs.[16,18] Graphite not only improves conductivity but also offers active sites for chemical reactions, making it effective for synthesising metallic nanoparticles.[22] In this sense, graphite was used to prepare platinum nanoparticles supported on graphite (PtNPs-G). A 20 mg $mL^{-1}$ aqueous solution of potassium hexachloroplatinate was mixed with 20 g of graphite powder overnight under constant stirring. After that, the solution was vacuum-filtered and dried in an oven at 60 °C. The resulting powder was named PtNPs-G and was characterised to confirm the presence of the platinum nanoparticles. Fig. 1A shows a simplified representation of the PtNPs-G material preparation process. This methodology used only water with no additional reducing agents to form the nanoparticles onto the graphite surface, emphasising the environmentally friendly production of this material.

To gain insight into the surface chemical composition of the proposed material SEM/EDX and XPS analysis were performed. Fig. 1B shows the SEM image of the PtNPs-G powder, indicating the characteristic flake morphology of graphite. Fig. 1C–E show the SEM image for a specific section of the powder and the corresponding EDX elemental mapping images of carbon and platinum, respectively, demonstrating the uniform distribution of carbon and the presence of PtNPs. The concentration of PtNPs is expected to be low since the reaction naturally occurs at the active sites of graphite without the need for any additional chemical agents.

Fig. 1F and G show the XPS C 1s spectra and Pt 4f spectra of PtNPs-G powder. To properly analyse the material, the XPS C 1s spectrum indicates a predominance of the asymmetric graphitic carbon peak at 284.5 eV, in accordance with the X-ray photoelectron emission.[24] It also shows three symmetric carbon satellites corresponding to C–C, C–O, and C═O. The results are consistent with previously reported XPS data for graphite material.[25] Furthermore, upon analysis of Fig. 1G, two main peaks are identified at 72.4 and 75.5 eV, corresponding to Pt $4f_{7/2}$ and $4f_{5/2}$, respectively. These results are consistent with previous reports in the literature,[26–28] indicating that these main doublets are characteristic of Pt(II). This demonstrates the formation of Pt nanoparticles in the form of platinum oxides, such as PtO and $Pt(OH)_2$, on the surface of the graphite powder. Note that the graphite acts as the reductant where platinum salt is reduced to form $Pt^0$ nanoparticles,

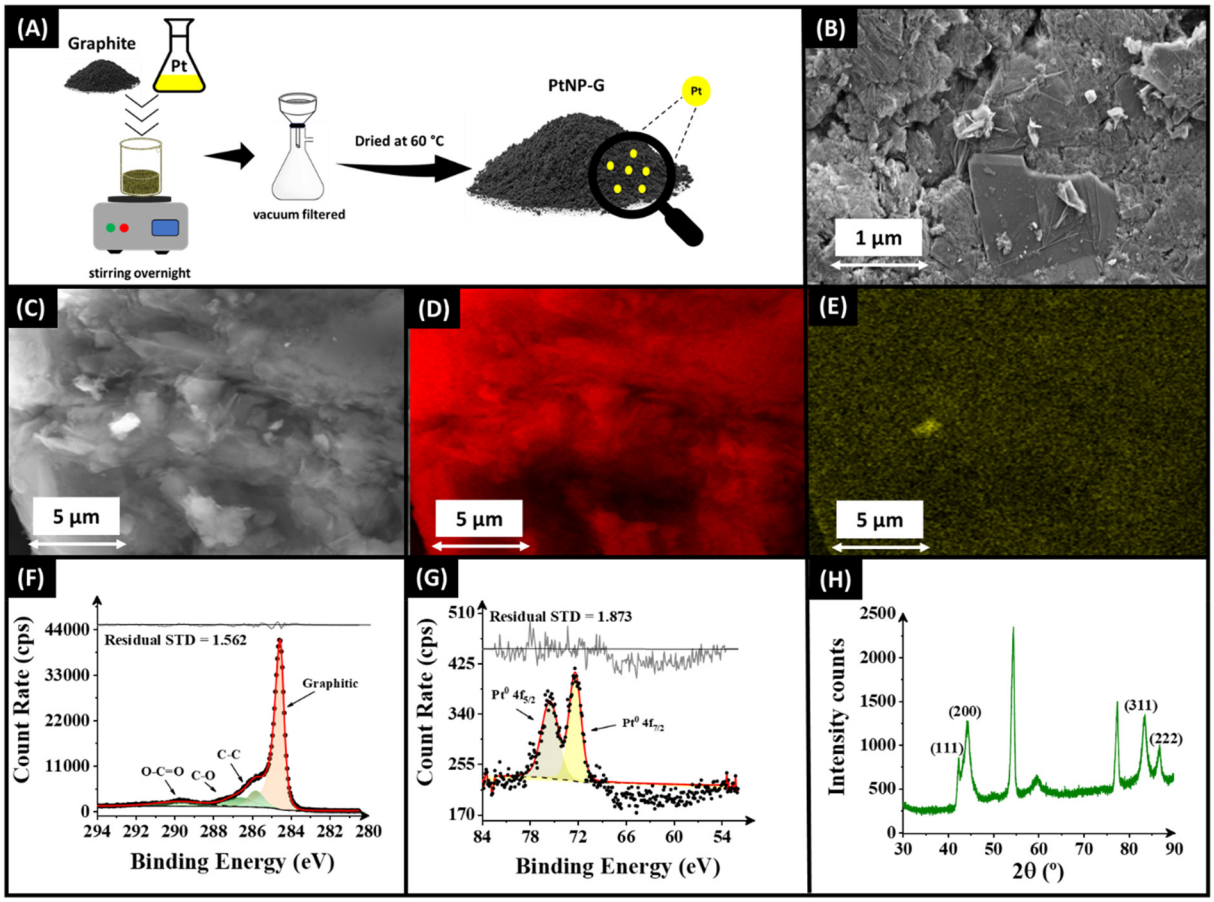


**Fig. 1** (A) Schematic representation of PtNPs-G production. (B) SEM and (C to E) EDX elemental mapping analysis of PtNPs-G additive manufactured electrode. (F) and (G) respective XPS data for graphite and PtNPs-G powders and (H) XRD pattern of PtNPs-G.

which then deposit onto the graphite surface, forming PtNPs-G. In this case, since the conditions are very mild, the oxidation of graphite is limited and surface based where the graphite develops a small number of oxygen-containing functional groups (*e.g.*, hydroxyl, carbonyl, or carboxyl groups) at the surface.

X-ray diffraction analysis confirmed the crystalline nature of the platinum nanoparticles. The XRD pattern of the synthesised platinum nanoparticles (PtNPs) on graphite is shown in Fig. 1H. This pattern shows four distinct Bragg reflection peaks that correspond to the lattice planes indexed to the face-centred cubic structure at (111), (200), (311), and (222) (JCPDS no. 89-7382).[29] The crystallite sizes were determined from the reflection peaks for PtNPs using the Debye-Scherrer eqn (1):[30,31]

$$D = k\lambda/(\beta \cos \theta) \quad (1)$$

where $D$ represents the average crystallite size calculated for all the reflection peaks, $k$ is the Scherrer constant commonly taken as 0.94,[32] $\lambda$ is the wavelength of X-ray source, $\beta$ is the corrected sample peak broadening or full width at half maximum (FWHM) and $\theta$ is the Bragg diffraction angle at peak position. Considering the four identified peaks, the average size of the PtNPs deposited on graphite using this approach was 145 ± 60 nm, confirming the nano-sized nature of the PtNPs.

A sustainable approach was used to create conductive filament using PtNPs-G (or graphite) as a conductive filler alongside CB in a ratio that optimises sustainability without compromising the electrochemical performance.[16,19] Additionally, a bio-based plasticiser castor oil and recycled poly(lactic acid) (rPLA) as the base polymer were used to maximise the sustainability of the final filament.[15,21] The production of the additive manufacturing filament was adapted from a previous report, with an increased overall carbon loading.[19] It involved adding rPLA (60 wt%), CB (18 wt%), PtNPs-G (or graphite, 9, 12, and 15 wt%), and castor oil (10 wt%) to a rheomixer chamber, and mixing at 190 °C for 5 minutes. The mixed material was utilised to produce an electrically conductive filament. The graphite and PtNPs-G(12%) filaments exhibited excellent flexibility, as shown in Fig. S1A and B.† Furthermore, the bulk resistance of filament was measured, allowing for comparisons between the filaments. The graphite filament exhibited a resistance of 40 ± 4 Ω cm$^{-1}$, while the PtNPs-G(12%) filament had a resistance of 42 ± 3 Ω cm$^{-1}$, indicating no significant change in

 

Fig. 2 Different infill pattern images from the PtNPs-G filament.

conductivity with the addition of PtNPs. However, these filaments both resulted in a notable enhancement in conductivity compared to literature values for CB-loaded filaments, which reported a resistance of 86 ± 5 Ω $cm^{-1}$.[15] Additionally, the filament developed in this study demonstrated superior conductivity to a previous report of CB/graphite filament, which showed a resistance of 88 ± 4 Ω $cm^{-1}$.[19] The improvement in this work is primarily due to the higher overall carbon loading (30 wt%), but it is important to note that this was achieved whilst not negatively affecting the flexibility and printability of the filaments.

Fig. 2 highlights the excellent printability of the PtNPs-G (12%) filament through printing different shapes with various infill patterns. In all cases, excellent print quality was obtained, indicating that these filaments in combination with additive manufacturing could be used to produce complex architectures to increase the available electroactive areas of electrodes and in turn improve the electrocatalytic performance of energy storage and conversion devices. These filaments were then used to print benchmark additively manufactured electrodes, which were characterised electrochemically.

### 3.2 Electrochemical characterisation of bespoke filaments

The electrochemical performance of simple lollipop electrodes printed from the bespoke graphite and PtNPs-G(12%) filaments was evaluated through voltammetric studies using the common outer- and inner-sphere redox probes, hexaammineruthenium(III) chloride $[Ru(NH_3)_6]^{3+}$ and $[Fe(CN)_6]^{4-}$. This electrode design was chosen to allow benchmarking against previously reported filaments. Table 1 summarises all the results obtained in the electrochemical characterisation study. In Fig. 3A, it is shown the scan rate study performed using the PtNPs-G(12%) additively manufactured electrode using cyclic voltammetry. This study applied scan rates ranged from 5 to 500 mV $s^{-1}$ against the near-ideal outer sphere redox probe $[Ru(NH_3)_6]^{3+}$ (1 mM in 0.1 M KCl), which allowed for the determination of the heterogeneous electron transfer rate constant

Table 1 Comparison of the electrochemical parameters using $[Ru(NH_3)_6]^{3+}$ and $[Fe(CN)_6]^{4-}$ redox probes

| | | Additively manufactured electrode | |
|---|---|---|---|
| Probe | Parameter | Graphite | PtNPs-G(12%) |
| $[Ru(NH_3)_6]^{3+}$ | $A_e$ ($cm^2$) | 0.53 ± 0.04 | 0.63 ± 0.03 |
| | $\Delta E_p$ (mV) | 124 ± 3 | 110 ± 2 |
| | $k^0$ (cm $s^{-1}$) | 1.75 (±0.06) × $10^{-3}$ | 2.05 (±0.07) × $10^{-3}$ |
| | $-I_p^c$ (μA) | 94 ± 7 | 115 ± 3 |
| $[Fe(CN)_6]^{4-}$ | $I_p^a$ (μA) | 74 ± 19 | 89 ± 3 |
| | $\Delta E_p$ (mV) | 192 ± 63 | 152 ± 13 |

($k^0$) and the real electrochemical surface area ($A_e$). The findings indicated that incorporating PtNPs into graphite to create the conductive filament resulted in better performance compared to a graphite filament in terms of $k^0$ and $A_e$ values (Table 1). The $k^0$ of the PtNPs-G(12%) electrode was found to be 2.05 (±0.07) × $10^{-3}$ cm $s^{-1}$, whereas the graphite electrode had a $k^0$ of 1.75 (±0.06) × $10^{-3}$ cm $s^{-1}$. Additionally, there is a clear increase in the electrochemical surface area from 0.53 ± 0.04 $cm^2$ for the graphite electrode to 0.63 ± 0.03 $cm^2$ with the PtNPs-G(12%) electrode, which is attributed to the presence of PtNPs. Furthermore, a comparison of the cyclic voltammetry performed for both graphite and PtNPs-G(12%) at 50 mV $s^{-1}$ against $[Ru(NH_3)_6]^{3+}$ (1 mM in 0.1 M KCl), Fig. 3B, demonstrated enhancements in cathodic peak current ($-I_p^c$) and peak-to-peak separation ($\Delta E_p$), also summarised in Table 1.

The electrochemical performance of the bespoke filament was also evaluated after activation in 0.5 M NaOH testing it against the inner-sphere redox probe $[Fe(CN)_6]^{4-}$ (1 mM in 0.1 M KCl). Fig. 3C shows the cyclic voltammograms (50 mV $s^{-1}$) obtained using PtNPs-G(12%) and graphite electrodes after activation. The results indicate a significant improvement in the $\Delta E_p$, with the PtNPs-G(12%) filament producing a value of 152 (±13) mV compared to 192 (±63) mV for the graphite electrode. Also, Table 1 shows enhancement in the anodic peak current ($I_p^a$) compared to the graphite electrode. This suggests a substantial improvement in electrochemical performance due to the presence of the nanoparticles. Fig. S2† shows the results of scan rate study using $[Ru(NH_3)_6]^{3+}$ for graphite electrode and the results using $[Fe(CN)_6]^{4-}$ for PtNPs-G(12%) and graphite electrodes.

The Nyquist plots obtained through electrochemical impedance spectroscopy (EIS) in $[Fe(CN)_6]^{4-/3-}$ (0.1 M KCl) for both additive manufactured electrodes are presented in Fig. 3D. It is demonstrated from Fig. 3D that both systems produced slightly similar charge-transfer resistances ($R_{ct}$). However, it is interesting to note that there was a significant improvement in solution resistance ($R_s$) for the PtNPs-G(12%) electrode. This indicates that the resistance introduced into the system is lower for the PtNPs-G(12%), measuring at 153 (±5) Ω compared to 358 (±70) Ω for the graphite electrode. This characterisation has shown how the presence of PtNPs improved the electrochemical properties of the additive manufactured electrodes and demonstrates the further potential application of the PtNPs-G(12%) electrode.

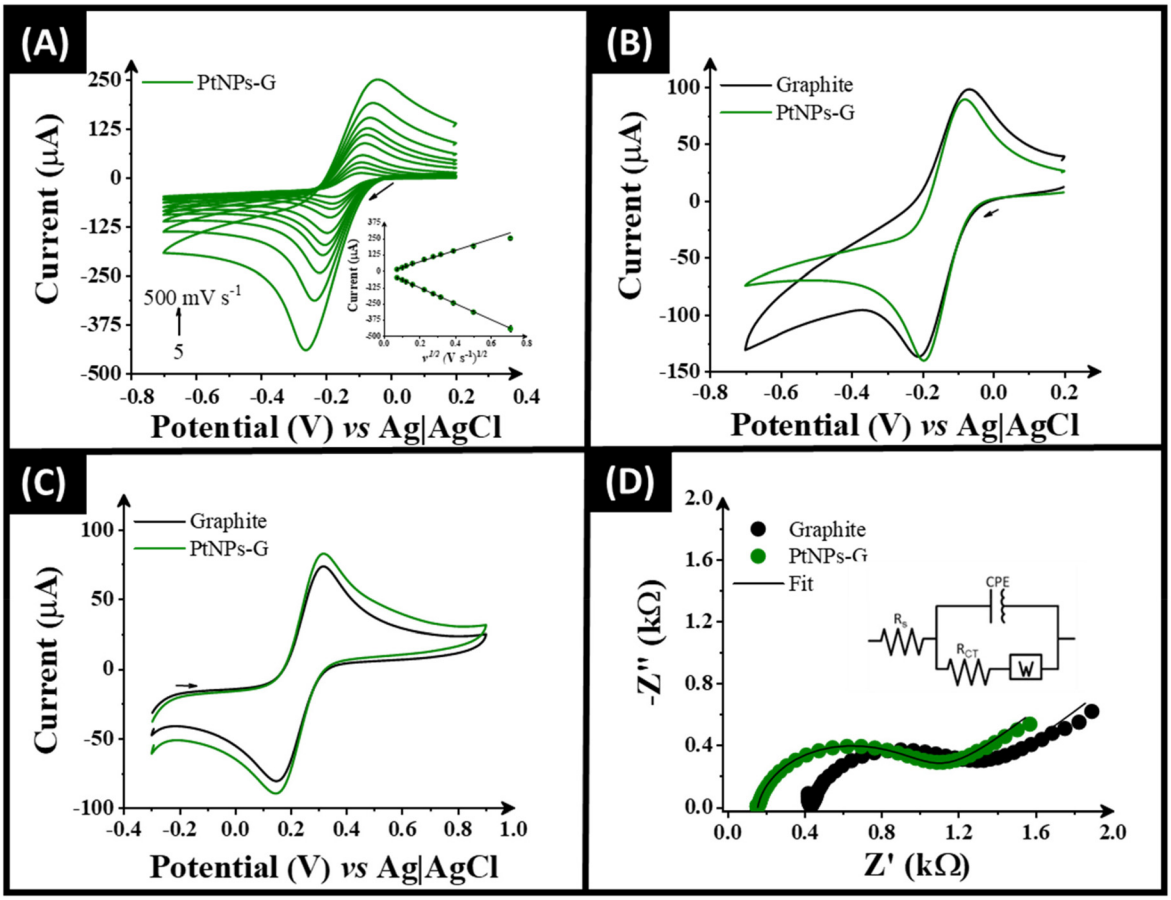


**Fig. 3** (A) Scan rate study (5–500 mV $s^{-1}$) with $[Ru(NH_3)_6]^{3+}$ (1 mM in 0.1 M KCl) performed in the PtNPs-G(12%) as the WE. Inset: the Randles–Ševčík plot. (B) CVs at 50 mV $s^{-1}$ of $[Ru(NH_3)_6]^{3+}$ and (C) $[Fe(CN)_6]^{4-/3-}$ comparing the PtNPs-G(12%) electrode with the Graphite electrode. (D) EIS Nyquist plots of $[Fe(CN)_6]^{4-/3-}$ comparing PtNPs-G(12%) with graphite. Inset: the proposed equivalent circuit.

### 3.3 Electrocatalytic activity towards the hydrogen evolution reaction

The electrochemically active surface area (ECSA) is an important factor that can influence the electrocatalytic activity of a material as it provides a quantitative measure of the active surface available for electrochemical reactions.[33,34] ECSA was estimated based on the double-layer capacitance ($C_{dl}$),[33] which was measured using CV experiments in the range of +0.15 to +0.25 V, where a non-faradaic process occurs. Fig. S3† shows the results from CV studies for the electrodes used in this work. Based on these results, $I_p$ *vs.* Scan Rate was next plotted at the potential of +0.20 V for each electrode, as represented in Fig. S4.† Using the absolute values of the slopes of the linear fits to the data obtained from Fig. S4,† the double-layer capacitance of the process is calculated. ECSA was calculated using the following:[35]

$$\mathrm{ECSA} = \frac{C_{dl}}{C_s} \quad (2)$$

where the term $C_s$ is the specific capacitance (34 μF $cm^{-2}$).[36] Table 2 shows the calculated $C_{dl}$ and ECSA values for each additive manufactured electrode studied and for a polycrystalline platinum electrode that was used for comparative purposes. The results show that there were no remarkable changes in the ECSA value among the additive manufactured electrodes used in this work. While a higher surface area is generally expected to increase the number of active sites, the effectiveness of the ECSA depends on the intrinsic activity of these sites. In other words, the efficiency of the hydrogen evolution reaction relies on the activity of each individual active site, which determines how effectively it facilitates the reaction.[37]

**Table 2** Calculated double-layer capacitance and ECSA for the additive-manufactured electrodes developed compared to standard platinum electrode

| Electrode | $C_{dl}$/μF | ECSA/$cm^2$ |
|---|---|---|
| Pt | 7.3 ± 2.0 | 0.21 ± 0.01 |
| Graphite | 7.0 ± 0.3 | 0.21 ± 0.05 |
| PtNPs-G(9%) | 5.7 ± 0.6 | 0.17 ± 0.02 |
| PtNPs-G(12%) | 5.1 ± 0.2 | 0.15 ± 0.02 |
| PtNPs-G(15%) | 6.6 ± 0.1 | 0.19 ± 0.04 |

Next, the electrocatalytic activity of the proposed additive manufactured electrodes was evaluated towards the hydrogen evolution reaction. To this end, linear sweep voltammetry

 

(LSV) measurements were performed. In this study, the additive manufactured electrodes were used as working electrodes alongside a Reversible Hydrogen Electrode (RHE) as reference and a nichrome wire as counter electrodes, respectively. Fig. 4 shows all the results obtained, which are expressed in terms of current density (mA $cm^{-2}$) *vs.* potential, as per the results of ECSA. First, the effect of polishing the electrodes with emery paper was evaluated. As shown in Fig. 4A, this approach enhanced the catalytic performance of the proposed electrodes. The improvement is likely similar to the effect observed when activating in 0.5 M NaOH,[15,38] where the removal of non-conductive material exposed more of the conductive materials (CB and PtNPs-G or Graphite), facilitating electrochemical reactions at the electrode surface. We also investigated the effect of NaOH activation (data not shown), but the results were less favourable for hydrogen evolution. This was likely ineffective because the potential applied during the chronoamperometry experiment for the activation may have triggered premature hydrogen evolution. This early hydrogen evolution could have compromised the electrocatalytic material's effectiveness in the HER experiment. The PtNPs-G(12%) polished electrode showed improved HER activity compared to the unpolished electrode, with an onset HER potential of −0.04 V (*vs.* RHE) compared to −0.15 V (*vs.* RHE) for the unpolished electrode. Based on these results, all subsequent experiments were focused exclusively on the polished electrodes. In the literature, most additive manufactured electrodes toward the HER are coated post-print, which adds an extra manufacturing step. Even so, the bespoke PtNPs-G(12%) filament showed enhanced performance compared to additive manufactured electrodes coated with $MoS_{3-\delta}$ reporting −0.2 V (*vs.* RHE)[39] and Ni–$MoS_2$ reporting −0.14 V (*vs.* RHE).[40] When compared to the few bespoke filaments reported previously, such as a PLA filament loaded with $MoSe_2$ or with commercial Pt/C catalyst which gave onset potentials of −0.30 V (*vs.* RHE) and −0.09 V (*vs.* RHE) respectively,[18] we can see that our bespoke filament is a significant advancement in additive manufacturing towards the HER. Furthermore, Table S1† shows a comparison between the bespoke PtNPs-G(12%) additive manufactured electrodes and others reported in the literature, where the pro-

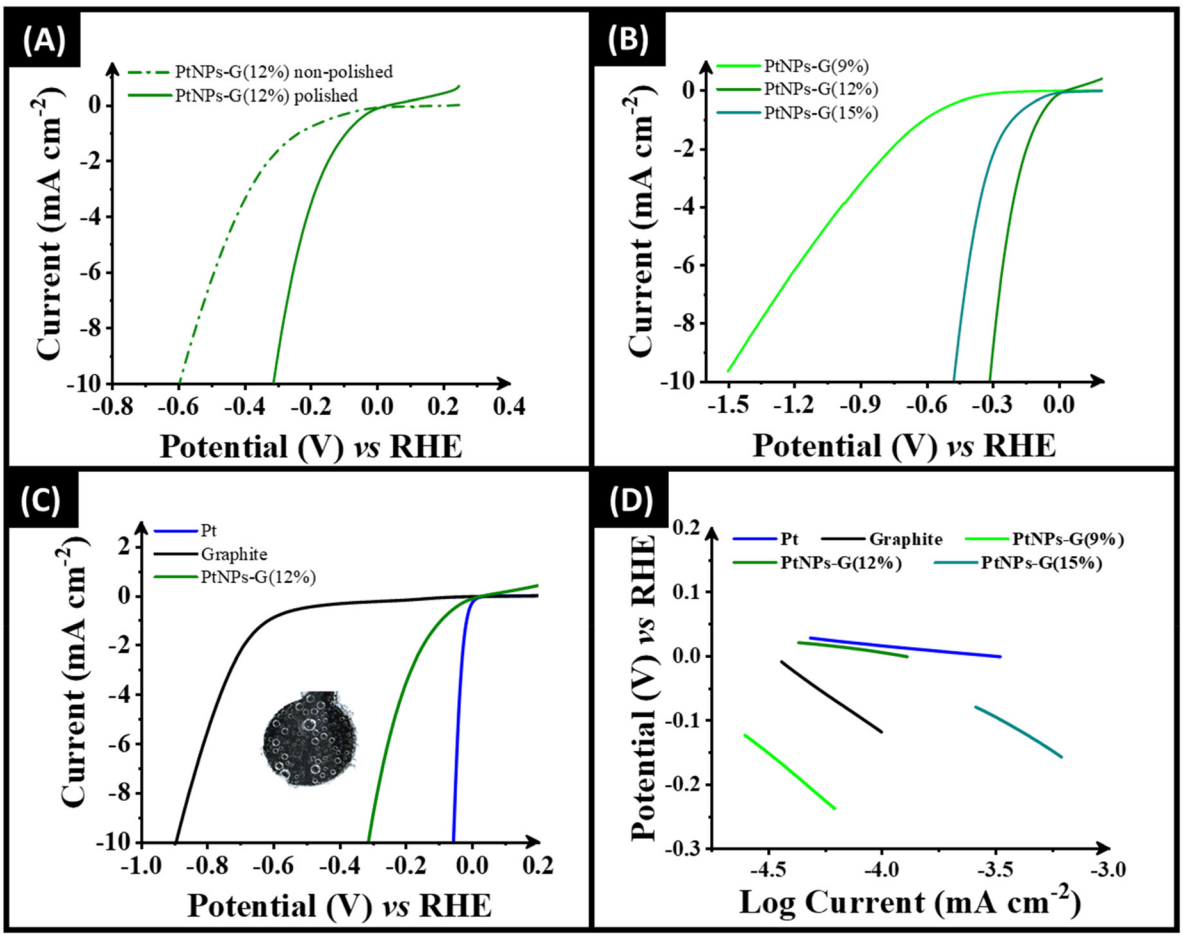


**Fig. 4** (A) Linear sweep voltammetry showing HER activity of polished and non-polished PtNPs-G(12%). (B) LSV comparing additive manufactured electrode with different PtNPs-G loadings (9%, 12%, and 15%) and (C) LSV of a polycrystalline platinum electrode, polished Graphite, and polished PtNPs-G(12%) showing HER activity. Inset: an image of the PtNPs-G(12%) as the working electrode, which is bubbling. Solution composition: 0.5 mol $L^{-1}$ $H_2SO_4$; scan rate ($v$): 10 mV $s^{-1}$. (D) Tafel slopes corresponding to the faradaic regions of the LSVs shown in (B) and (C).

posed additively manufactured electrode performs excellently towards HER.

The influence of the varying amounts of PtNPs-G was also investigated for HER. As shown in Fig. 4B, the electrode with 12% PtNPs-G outperformed those with 9% and 15% with a current density of −9.12 mA $cm^2$ and −0.3 V (*vs.* RHE), while PtNPs-G at 9% and 15% achieved this magnitude of current density at more negative potentials corresponding to −1.45 V and −0.46 V, respectively. When comparing the 12% PtNPs-G electrode to the one with 9% PtNPs-G, it is evident that increasing the amount of PtNPs-G enhanced the catalytic activity providing more catalytic sites available for hydrogen evolution reaction.[18] The onset potential for the 9% PtNPs-G electrode was −0.48 V (*vs.* RHE), indicating a 12-fold decrease in HER performance compared to the 12% PtNPs-G electrode, which had a significantly more favourable onset potential of −0.04 V (*vs.* RHE). Increasing the quantity of PtNPs-G to 15% yielded better results than 9% but was still inferior to the performance for 12%, with an onset potential of −0.08 V (*vs.* RHE). This is possibly attributed also to the higher graphite content in the filament. As demonstrated by our research group in a previous study,[16] higher graphite concentration in the filament can weaken the conductive network due to the size difference between small carbon black particles and large graphite flakes. A balance of both types is needed for optimal conductivity, as too many large flakes reduce connectivity.

Fig. 4C compares the performance of the PtNPs-G(12%) with polycrystalline platinum and additive manufactured graphite electrodes. Pt electrode demonstrates exceptional HER activity, with an onset potential at 0.01 V (*vs.* RHE). PtNPs-G(12%) electrode shows a substantial enhancement in HER activity, achieving the most positive onset potential among the additive manufactured electrodes at −0.04 V (*vs.* RHE). In contrast, graphite electrode exhibits the largest onset potential of −0.52 V (*vs.* RHE), which can be attributed to the lack of catalytic materials besides the conductive carbon in the PLA matrix, leading to poor HER efficiency. The improvements observed with PtNPs-G(12%) are likely due to the Triple Phase Boundary (TPB) effect, where solid, liquid, and gas phases interact to enable effective electrochemical reactions. The platinum nanoparticles (PtNPs) created more active sites at the TPBs essential for catalysis. This enhances interactions among the gas, liquid, and solid phases, improving mass transfer, reactant distribution, and conversion efficiency.[41,42]

It is essential to analyse the mechanism of the hydrogen evolution reaction. To achieve this, the Tafel slopes were evaluated (Fig. 4D) interpreting the Tafel slope values, we could determine the rate-limiting step for each electrode studied. It is described in the literature that in an acidic medium, the HER typically occurs through three main steps. The first one is the adsorption of hydrogen (H) on the surface of the catalyst, known as the Volmer reaction, which is characterised with a Tafel slope of 120 mV $dec^{-1}$. The second step varies depending on the nature of the electrocatalysis. It can involve the reaction of an adsorbed H atom with a proton ($H^+$) from the electrolyte, called the Heyrovsky reaction, which has a slope of 40 mV $dec^{-1}$. Alternatively, it can involve the reaction between two adsorbed H atoms, known as the Tafel reaction, with a slope of 30 mV $dec^{-1}$, resulting in the formation of a hydrogen molecule ($H_2$).[18,43] Based on the results obtained, Pt electrode demonstrated the expected Volmer–Tafel mechanism,[18,44] exhibiting a Tafel slope of 35 mV $dec^{-1}$ with an overpotential ($\eta$) at 10 mA $cm^{-2}$ (mV *vs.* RHE) of −28 mV.[45] Comparing with the additive manufactured electrodes, PtNPs-G(12%) electrode showed the best Tafel slope of 46 mV $dec^{-1}$, indicating satisfactory HER catalysis following a Volmer–Heyrovsky mechanism with an $\eta$ of −312 mV. On the other hand, graphite, PtNPs-G (9%), and PtNPs-G(15%) electrodes displayed Tafel slopes and $\eta$ of 246, 293, and 208 mV $dec^{-1}$ and −693, −1050, and −471 mV, respectively. For these electrodes, the initial adsorption step (Volmer reaction) was identified as the rate-limiting factor, suggesting that they exhibit poor HER catalysis.

To evaluate the stability of the proposed electrode in relation to the hydrogen evolution reaction, Fig. 5 shows the results for LSV experiments conducted 1000 times at a scan rate of 50 mV $s^{-1}$ and chronoamperometry studies performed for 7 hours at −0.3 V (*vs.* RHE). Fig. 5A illustrates a reduction in the HER activity with a 1.5-fold increase in the onset potential from the 1$^{st}$ to the 100$^{th}$ scan. On the other hand, from the 100$^{th}$ to the 1000$^{th}$ scan, Fig. 5A shows a slight improvement in HER activity, resulting in a 1.14-fold increase. These shifts may be attributed to water ingress into the electrode, which compromises its stability. Previous research on additive manufactured electrodes made of PLA has shown that these electrodes can absorb solutions after prolonged exposure. This ingress can lead to changes in electrochemical properties, such as current and electroactive surface area, as well as minor dimensional alterations that may affect the structural integrity of the electrode in long-term applications.[46] This is further illustrated in Fig. 5B, where the electrode exhibited a significant change in current after 4 hours of continuous measurement, with current values decreasing by 22%. This suggested that water ingress likely altered the properties of the electrode.

Overall, the results indicate that despite the challenges of long-term stability, primarily attributed to the composition of the base polymer, the proposed electrode provides significant advantages in efficiency for the hydrogen evolution reaction. It is prudent to consider this work against others. Reported in this paper, we have produced platinum nanoparticles on graphite flakes using an eco-friendly aqueous synthesis and no additional reagents. This was used to make a bespoke filament from recycled PLA and bio-based castor oil, using only 5 minutes of thermal mixing and no solvents. The filament showed excellent printability and performance towards the production of green hydrogen compared to previously reported materials (Tables S1 and S2†). For example, phosphorus-doped activated carbon is used as a support for Pt catalysts.[13] They synthesised phosphorus-doped activated carbon by introducing phosphorus into activated carbon and mixing it at 500 degrees Celsius for 3 h, after which, the mixture is heating for 1 h at 1200 degrees Celsius. This is then modified dissolving chloroplatinic acid in ethylene glycol with phosphorus-doped

 

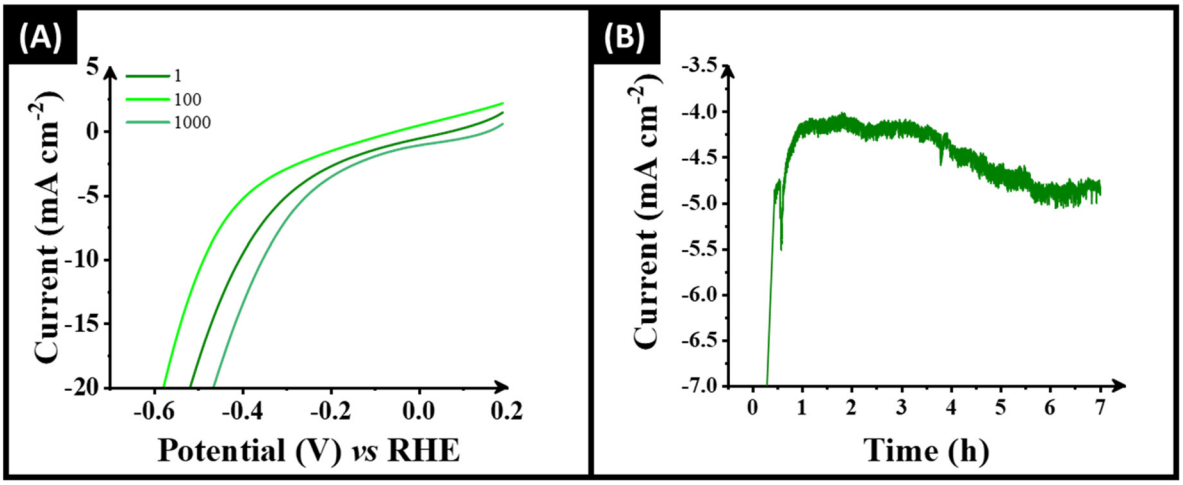


**Fig. 5** Stability examination of PtNPs-G(12%) *via* (A) LSV (scan rate: 50 mV $s^{-1}$) performed between the potential range of +0.2 to −0.6 V (*vs.* RHE), repeated for 1000 cycles. (B) Chronoamperometry for 7 hours at −0.30 V with PtNPs-G(12%) as WE (*vs.* RHE).

activated carbon using ultrasonic dispersion followed heating at 140 degrees Celsius for 3 h. A large amount of energy is used to produce a phosphorus-doped activated carbon is used as a support for Pt catalysts but it is not sustainable in practice.[13] Zhang *et al.*[12] report platinum atoms onto the 2D material MXene but they used HF for 48 h at 55 degrees Celsius to make the MXene which is then delaminated using organic solvent for 24 h. Last, the material is electrochemical exfoliated and atom trapping strategy.[12] Overall, an un-green strategy where the process itself is harsh, energy-intensive, and chemically toxic. In summary, our approach provides a green chemistry approach where we have detailed an eco-friendly aqueous synthesis and no additional reagents (Table S2†).

## 4. Conclusions

The study successfully demonstrates the green synthesis of platinum nanoparticles supported on graphite (PtNPs-G) for the creation of Pt doped additive manufacturing filament. This sustainable approach combines recycled PLA, carbon black, bio-based plasticiser castor oil, and PtNPs-G to create a novel conductive filament, achieving enhanced conductivity and electrochemical performance. Electrodes printed from this filament exhibited improved electrochemical behaviour towards both outer- and inner-sphere redox probes. Notably, the inclusion of 12% PtNPs reduced the $\Delta E_p$ from 124 (±3) mV to 110 (±2) mV and increased the $k^0$ from 1.75 (±0.06) × $10^{-3}$ cm $s^{-1}$ to 2.05 (±0.07) × $10^{-3}$ cm $s^{-1}$ and the $A_e$ from 0.53 (±0.04) $cm^2$ to 0.63 (±0.03) $cm^2$ when using hexaammineruthenium(III) chloride as a redox probe.

PtNPs-G(12%) electrode demonstrated optimised electrocatalytic activity, achieving an onset HER potential of −0.04 V (*vs.* RHE), a significant improvement over the graphite electrode (−0.52 V). PtNPs-G(12%) electrode followed a Volmer–Heyrovsky mechanism, as indicated with a Tafel slope of 46 mV $dec^{-1}$ and an overpotential of −312 mV at a current density of 10 mA $cm^{-2}$. Stability tests over 1000 scans and 7 hours of chronoamperometry showed good stability, although some performance decline was observed, likely due to water ingress into the PLA matrix. Overall, the development of PtNPs-G-based filaments emphasises the potential of additive manufacturing to produce sustainable, high-performance electrodes for electrochemical applications. The optimised PtNPs-G(12%) electrode offers significant improvements in HER activity, making it a promising candidate for renewable energy technologies. Last, this approach relies on platinum, a precious and scarce metal, but our approach is to show proof-of-concept that one can utilise green chemistry with a suitable approach. Further work is suggested to replace platinum with other useful materials such as nickel sulphide for instance.

## Data availability

The data supporting this article have been included as part of the ESI.†

## Conflicts of interest

There are no conflicts of interest to declare.

## Acknowledgements

The authors would like to thank Chetna Tyagi for the acquisition of XRD data. We thank EPSRC (EP/W033224/1), Horizon Europe (101137990), CNPq (Conselho Nacional de Desenvolvimento Científico e Tecnológico) grants 140406/2021-2 and 401681/2023-8, INCT Nanovida (CNPq) grant 406079/2022-6, Fundação Coordenação de Aperfeiçoamento de

Pessoal de Nível Superior (CAPES-Print) grant 88887.836030/2023-00, FAPESP (Fundação de Amparo à Pesquisa do Estado de São Paulo) grant 2024/04116-8 for funding.



## References

1 N. Ma, W. Zhao, W. Wang, X. Li and H. Zhou, *Int. J. Hydrogen Energy*, 2024, **50**, 379–396.
2 M. Hermesmann and T. E. Müller, *Prog. Energy Combust. Sci.*, 2022, **90**, 100996.
3 R. Li, D. Zhou, J. Luo, W. Xu, J. Li, S. Li, P. Cheng and D. Yuan, *J. Power Sources*, 2017, **341**, 250–256.
4 A. Irshad and N. Munichandraiah, *ACS Appl. Mater. Interfaces*, 2017, **9**, 19746–19755.
5 U. Nations, The 17 Goals, **https://sdgs.un.org/goals**, (accessed 14/02/2025, 2025).
6 F. Kourougianni, A. Arsalis, A. V. Olympios, G. Yiasoumas, C. Konstantinou, P. Papanastasiou and G. E. Georghiou, *Renewable Energy*, 2024, **231**, 120911.
7 P. C. K. Vesborg, B. Seger and I. Chorkendorff, *J. Phys. Chem. Lett.*, 2015, **6**, 951–957.
8 C. C. L. McCrory, S. Jung, I. M. Ferrer, S. M. Chatman, J. C. Peters and T. F. Jaramillo, *J. Am. Chem. Soc.*, 2015, **137**, 4347–4357.
9 J. X. Wang, Y. Zhang, C. B. Capuano and K. E. Ayers, *Sci. Rep.*, 2015, **5**, 12220.
10 K. L. Zhou, Z. Wang, C. B. Han, X. Ke, C. Wang, Y. Jin, Q. Zhang, J. Liu, H. Wang and H. Yan, *Nat. Commun.*, 2021, **12**, 3783.
11 J. Scremin, I. V. Joviano dos Santos, J. P. Hughes, A. García-Miranda Ferrari, E. Valderrama, W. Zheng, X. Zhong, X. Zhao, E. J. R. Sartori, R. D. Crapnell, S. J. Rowley-Neale and C. E. Banks, *Nanoscale*, 2020, **12**, 18214–18224.
12 J. Zhang, Y. Zhao, X. Guo, C. Chen, C.-L. Dong, R.-S. Liu, C.-P. Han, Y. Li, Y. Gogotsi and G. Wang, *Nat. Catal.*, 2018, **1**, 985–992.
13 H. Chen, X. Luo, S. Huang, F. Yu, D. Li and Y. Chen, *J. Electroanal. Chem.*, 2023, **948**, 117820.
14 E. Bernalte, K. K. L. Augusto, R. D. Crapnell, H. G. Andrews, O. Fatibello-Filho and C. E. Banks, *RSC Appl. Interfaces*, 2025, **2**, 439–450.
15 R. D. Crapnell, I. V. S. Arantes, M. J. Whittingham, E. Sigley, C. Kalinke, B. C. Janegitz, J. A. Bonacin, T. R. L. C. Paixão and C. E. Banks, *Green Chem.*, 2023, **25**, 5591–5600.
16 K. K. L. Augusto, R. D. Crapnell, E. Bernalte, S. Zighed, A. Ehamparanathan, J. L. Pimlott, H. G. Andrews, M. J. Whittingham, S. J. Rowley-Neale, O. Fatibello-Filho and C. E. Banks, *Microchim. Acta*, 2024, **191**, 375.
17 R. M. Cardoso, C. Kalinke, R. G. Rocha, P. L. dos Santos, D. P. Rocha, P. R. Oliveira, B. C. Janegitz, J. A. Bonacin, E. M. Richter and R. A. A. Munoz, *Anal. Chim. Acta*, 2020, **1118**, 73–91.
18 J. P. Hughes, P. L. dos Santos, M. P. Down, C. W. Foster, J. A. Bonacin, E. M. Keefe, S. J. Rowley-Neale and C. E. Banks, *Sustainable Energy Fuels*, 2020, **4**, 302–311.
19 I. V. S. Arantes, R. D. Crapnell, E. Bernalte, M. J. Whittingham, T. R. L. C. Paixão and C. E. Banks, *Anal. Chem.*, 2023, **95**, 15086–15093.
20 E. Bernalte, R. D. Crapnell, R. El Azizi, K. K. L. Augusto and C. E. Banks, *Appl. Mater. Today*, 2025, **42**, 102578.
21 E. Sigley, C. Kalinke, R. D. Crapnell, M. J. Whittingham, R. J. Williams, E. M. Keefe, B. C. Janegitz, J. A. Bonacin and C. E. Banks, *ACS Sustainable Chem. Eng.*, 2023, **11**, 2978–2988.
22 R. K. Pandey, L. Chen, S. Teraji, H. Nakanishi and S. Soh, *ACS Appl. Mater. Interfaces*, 2019, **11**, 36525–36534.
23 E. Bernalte, R. D. Crapnell, O. M. A. Messai and C. E. Banks, *ChemElectroChem*, 2024, **11**, e202300576.
24 R. Blume, D. Rosenthal, J.-P. Tessonnier, H. Li, A. Knop-Gericke and R. Schlögl, *ChemCatChem*, 2015, **7**, 2871–2881.
25 R. I. R. Blyth, H. Buqa, F. P. Netzer, M. G. Ramsey, J. O. Besenhard, P. Golob and M. Winter, *Appl. Surf. Sci.*, 2000, **167**, 99–106.
26 P.-L. Kuo, W.-F. Chen, H.-Y. Huang, I. C. Chang and S. A. Dai, *J. Phys. Chem. B*, 2006, **110**, 3071–3077.
27 J. Prabhuram, T. S. Zhao, C. W. Wong and J. W. Guo, *J. Power Sources*, 2004, **134**, 1–6.
28 Z. Q. Tian, S. P. Jiang, Y. M. Liang and P. K. Shen, *J. Phys. Chem. B*, 2006, **110**, 5343–5350.
29 W. Ji, W. Qi, S. Tang, H. Peng and S. Li, *Nanomaterials*, 2015, **5**, 2203–2211.
30 I. S. Lopes, B. N. Oliveira de Moraes, S. de Souza Barreto, L. Le Joncour, C. Couteau, M. R. Franzolin and L. C. Courrol, *Mater. Chem. Phys.*, 2025, **333**, 130364.
31 J. S. Afolayan, A. M. Varney, J. C. Thomas, S. McLean and C. C. Perry, *Colloids Surf., B*, 2025, **245**, 114280.
32 J. I. Langford and A. J. C. Wilson, *J. Appl. Crystallogr.*, 1978, **11**, 102–113.
33 C. C. L. McCrory, S. Jung, J. C. Peters and T. F. Jaramillo, *J. Am. Chem. Soc.*, 2013, **135**, 16977–16987.
34 H. Su, X. Pan, S. Li, H. Zhang and R. Zou, *Carbon Energy*, 2023, **5**, e296.
35 P. Connor, J. Schuch, B. Kaiser and W. Jaegermann, *Z. Phys. Chem.*, 2020, **234**, 979–994.
36 M. Łukaszewski, M. Soszko and A. Czerwiński, *Int. J. Electrochem. Sci.*, 2016, **11**, 4442–4469.
37 C. Wei, S. Sun, D. Mandler, X. Wang, S. Z. Qiao and Z. J. Xu, *Chem. Soc. Rev.*, 2019, **48**, 2518–2534.
38 R. M. Cardoso, S. V. F. Castro, M. N. T. Silva, A. P. Lima, M. H. P. Santana, E. Nossol, R. A. B. Silva, E. M. Richter, T. R. L. C. Paixão and R. A. A. Muñoz, *Sens. Actuators, B*, 2019, **292**, 308–313.
39 C. Iffelsberger, S. Ng and M. Pumera, *Appl. Mater. Today*, 2020, **20**, 100654.
40 A. Ambrosi and M. Pumera, *ACS Sustainable Chem. Eng.*, 2018, **6**, 16968–16975.

 

41 K. K. Karuppanan, A. V. Raghu, M. K. Panthalingal, S. Ramanathan, T. Kumaresan and B. Pullithadathil, *J. Mater. Chem. A*, 2018, **6**, 12768–12781.
42 L. Mohapatra, L. Paramanik, S. Sabnam and S. H. Yoo, *Nanoscale*, 2024, **16**, 22099–22119.
43 A. P. Murthy, J. Theerthagiri and J. Madhavan, *J. Phys. Chem. C*, 2018, **122**, 23943–23949.
44 B. Yu, X. Wang, F. Qi, B. Zheng, J. He, J. Lin, W. Zhang, Y. Li and Y. Chen, *ACS Appl. Mater. Interfaces*, 2017, **9**, 7154–7159.
45 R. G. Compton and C. E. Banks, *Understanding Voltammetry*, World Scientific, 4th edn, 2025.
46 R. J. Williams, T. Brine, R. D. Crapnell, A. G.-M. Ferrari and C. E. Banks, *Mater. Adv.*, 2022, **3**, 7632–7639.